Many-Body Resonances in the Avalanche Instability of Many-Body Localization

Hyunsoo Ha◉,[1] Alan Morningstar◉,[1,2] and David A. Huse◉[1]

[1]*Department of Physics, Princeton University, Princeton, New Jersey 08544, USA*
[2]*Department of Physics, Stanford University, Stanford, California 94305, USA*

Many-body localized (MBL) systems fail to reach thermal equilibrium under their own dynamics, even though they are interacting, nonintegrable, and in an extensively excited state. One instability toward thermalization of MBL systems is the so-called "avalanche," where a locally thermalizing rare region is able to spread thermalization through the full system. The spreading of the avalanche may be modeled and numerically studied in finite one-dimensional MBL systems by weakly coupling an infinite-temperature bath to one end of the system. We find that the avalanche spreads primarily via strong many-body resonances between rare near-resonant eigenstates of the closed system. Thus we find and explore a detailed connection between many-body resonances and avalanches in MBL systems.

Introduction.—Many-body localized (MBL) systems are a class of isolated many-body quantum systems that fail to thermalize due to their own unitary dynamics, even though they are interacting, nonintegrable, and extensively excited [1–7]. This happens for one-dimensional systems with short-range interactions in the presence of strong enough quenched randomness, which yields a thermal-to-MBL phase transition of the dynamics. In the MBL phase, there are an extensive number of emergent localized conserved operators [8–11].

One instability of the MBL phase that is believed to play a central role in the asymptotic, long-time, infinite-system MBL phase transition is the "avalanche" [12–15]. Rare locally thermalizing regions necessarily exist due to the randomness. Starting from such a rare region, this "thermal bubble" spreads through the adjacent typical MBL regions until the relaxation rate of the adjacent spins becomes smaller than the many-body level spacing of the thermal bubble, in which case the avalanche halts. If the strength of the randomness is insufficient, the relaxation rate remains larger than the level spacing and the avalanche does not stop: the full system then slowly thermalizes and is no longer in the MBL phase (although it is in a prethermal-MBL regime [16,17]).

The avalanche has been numerically simulated in small systems [16,18–22] and experimentally probed [23]. Recent work shows that the instability of MBL to avalanches occurs at much stronger randomness than had been previously thought [16,21]. This leaves a large intermediate prethermal-MBL regime in the phase diagram between the onset of MBL-like behavior in small samples (or correspondingly short times) and the asymptotic MBL phase transition. Clear numerical evidence has been obtained for many-body resonances being an important part of the physics in the near-thermal part of this regime [16,17,24–30], while no such evidence for the expected thermalizing rare regions has been found yet. In the part of this intermediate prethermal regime that is farther from the thermal regime, it remains unclear what the primary mechanism that leads to thermalization is for samples larger than those that can be diagonalized.

In this Letter, we explore how an avalanche spreads through typical MBL regions for systems that are near the avalanche instability. In particular, we uncover explicit connections between many-body resonances and avalanches. We do not simulate the rare region that initiates the avalanche. Instead, we assume a large avalanche is spreading, and that we may model that as an infinite-temperature bath (see Fig. 1) weakly coupled to one end of our MBL spin chain [16,21] (similar settings were also considered for studying transport [31–34]). We find that particular many-body "near-resonances" of the closed system play a key role in facilitating the avalanche. These near-resonances are the dominant process by which the bath at one end of the chain thermalizes the other end of the chain and thus propagates the avalanche.

Model.—Our model consists of a chain of L spin-1/2 degrees of freedom. The dynamics of the closed system is given by the random-circuit Floquet MBL model of Ref. [16], which has unitary Floquet operator $\hat{U}_F$. The disorder strength in this model is given by the parameter α, with localization occurring at large α [see the Supplemental Material (SM) [35] for model details]. To investigate avalanche spreading, we weakly connect an infinite-temperature Markovian bath to spin L at the right end of the system [16,21]. The quantum state of this open system is the density matrix $\hat{\rho}(t)$.
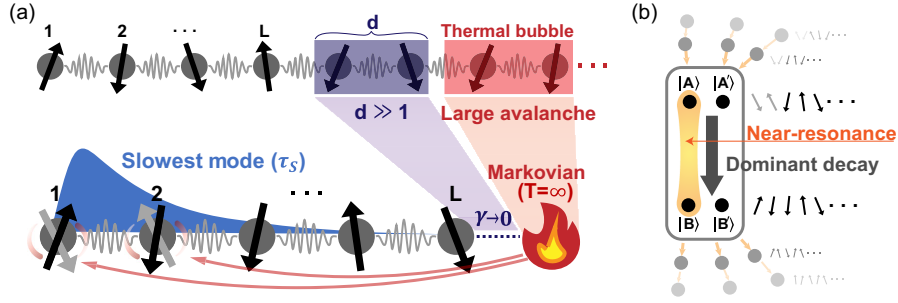
FIG. 1. (a) The avalanche model. We model the large avalanche (seeded by a bare thermal rare region) spreading, but still far away ($d \gg 1$) by connecting the Markovian infinite-temperature bath in the weak-coupling limit with the one-dimensional MBL system of length L spins. Specifically, we analyze the decay of the slowest mode ($\hat{\tau}_S$), which is localized near the end of the system farthest from the bath; $\hat{\tau}_S$ is a "localized integral of motion" in the MBL phase. (b) Schematic decay of $\hat{\tau}_S$. A large fraction of the probability current in the decay of $\hat{\tau}_S$ passes through four eigenstates associated with a rare near-resonance.

In our open-system Floquet model, the bath is represented by the superoperator S_{bath} that acts once each time period:

$$S_{\text{bath}}[\hat{\rho}] = \frac{\hat{\rho}}{1+3\gamma} + \frac{\gamma}{1+3\gamma}\sum_{j=1}^{3}\hat{E}_j\hat{\rho}\hat{E}_j^\dagger, \qquad (1)$$

where $(\hat{E}_1, \hat{E}_2, \hat{E}_3) = (\hat{X}_L, \hat{Y}_L, \hat{Z}_L)$ are the jump operators acting on the last spin at site L. We will take the weak-coupling limit $\gamma \to 0$, representing the exponentially weak coupling of spin L to the distant thermal rare region. The open-system Floquet superoperator S_{period} that takes our system through one time period is $S_{\text{period}}[\hat{\rho}(t)] = S_{\text{bath}}[\hat{U}_F\hat{\rho}(t)\hat{U}_F^\dagger]$. The time evolution of the system's state is given by

$$\hat{\rho}(t) = \hat{\mathbb{1}}/2^L + p_1 e^{-r_1 t}\hat{\tau}_1 + \sum_{k\geq 2}p_k e^{-r_k t}\hat{\tau}_k, \qquad (2)$$

where e^{-r_k} is the kth largest eigenvalue of S_{period} with eigenoperator $\hat{\tau}_k$. Note that the largest (0th) eigenvalue is 1 and is nondegenerate when $\gamma > 0$, with eigenoperator proportional to the identity, which is the steady state of this system. The mode with the slowest relaxation for $\gamma > 0$ is $\hat{\tau}_S := \hat{\tau}_1$, which relaxes with rate $r_S := \text{Re}(r_1)$. The relaxation rate r_S is proportional to γ, and we work to first order in γ [16,21].

Relaxation of the slowest mode.—In the weak-coupling limit, one can obtain $\hat{\tau}_S$ as a superposition of the diagonal terms $|n\rangle\langle n|$, where $|n\rangle$ are the eigenstates of the closed system such that $\hat{U}_F|n\rangle = e^{i\theta_n}|n\rangle$. When $\gamma = 0$, then $|m\rangle\langle n|$ are eigenoperators of S_{period} with eigenvalues $e^{i(\theta_m-\theta_n)}$, so all diagonal terms $|n\rangle\langle n|$ are degenerate, with $r_k = 0$. Therefore, in the $\gamma \ll 1$ limit, one can obtain $\hat{\tau}_S$ in degenerate perturbation theory by diagonalizing the (super) operator $S[\hat{\rho}] := \frac{1}{3}\sum_{j=1}^{3}\hat{E}_j\hat{\rho}\hat{E}_j^\dagger$ in this degenerate subspace [21], where the matrix elements are

$$S_{mn} = \langle m|S[|n\rangle\langle n|]|m\rangle = \frac{1}{3}\sum_{j=1}^{3}|\langle m|\hat{E}_j|n\rangle|^2. \qquad (3)$$

Note that this is a symmetric stochastic matrix with real eigenvalues. In particular, $\hat{\tau}_S = \sum_n c_n|n\rangle\langle n|$ where $\vec{c}$ is the eigenvector of S with the smallest spectral gap Γ from the steady state $[\sum_m S_{nm}c_m = (1-\Gamma)c_n]$. The relaxation rate is $r_S = 3\gamma\Gamma$. We normalize $\hat{\tau}_S$ so $\text{Tr}\{\hat{\tau}_S^2\} = \sum_n|c_n|^2 = 2^L$.

Naively, the slowest mode is the local integral of motion (LIOM) that is farthest from the bath. More precisely $\hat{\tau}_S$ is a traceless superposition of projectors on to the eigenstates of the closed system. Among such operators, it is the one with the smallest weight of Pauli strings with nonidentity at site L [35]. It is a LIOM that is indeed localized far from the bath, but it is different in detail from the ℓ bits and LIOMs of Refs. [8–10,36].

The latest time dynamics are determined by $\hat{\tau}_S$, with $\hat{\rho}(t) \simeq \hat{\mathbb{1}}/2^L + p_S e^{-r_S t}\hat{\tau}_S$ for any initial conditions that contain $\hat{\tau}_S$. This assumes a nonzero gap between (r_1/γ) and (r_2/γ), which is the case for all samples examined. We can view the slow relaxation of $\hat{\tau}_S$ in terms of probability currents that flow between the eigenstates of the isolated system, leading to the final $\hat{\rho} = \hat{\mathbb{1}}/2^L$ equilibrium where all eigenstates have equal weight. Specifically, we may quantify the contribution D_{mn} of the pair of eigenstates m, n to the relaxation of $\hat{\tau}_S$ as

$$D_{mn} := S_{mn}(c_m - c_n)^2 \geq 0. \qquad (4)$$

One can show [35] that the relaxation rate of $\hat{\tau}_S$ is given by the sum of the contributions from all pairs of eigenstates of the closed system:

$$\sum_{m<n}D_{mn} = \Gamma\,\text{Tr}\{\hat{\tau}_S^2\} = 2^L\Gamma. \qquad (5)$$

We find the pair of eigenstates $|\mu\rangle$, $|\nu\rangle$ that gives the strongest contribution to the relaxation of $\hat{\tau}_S$ by finding the pair with the largest D_{mn}. We quantify the fraction of the full relaxation that is due to this pair by the ratio $R \equiv D_{\mu\nu}/(2^L\Gamma)$. The distribution of R over disorder realizations and for different system sizes is shown in Fig. 2, both for the thermal regime and for the MBL regime near
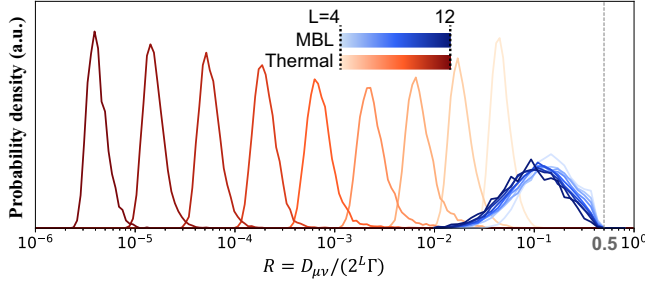
FIG. 2. Probability distribution over samples of the ratio $R = D_{\mu\nu}/(2^L\Gamma)$ (see text). In the thermal regime (dark red to yellow), the ratio exponentially decays with increasing L. In comparison, R barely drifts with L for the MBL case (blue). We observe that R never exceeds the value 0.5 (gray dashed line), which is explained with the minimal model in the main text. In this figure, we used $\alpha = 30$ and $\alpha = 1$ for MBL and thermal regimes, respectively.

the avalanche instability. In the thermal regime, R decreases exponentially with increasing L, indicating that many pairs of eigenstates are contributing similar amounts to the relaxation of the slowest mode, which is as should be expected for this thermal regime.

In the MBL regime, we find that this pair of eigenstates contributes an order-1 fraction that does not decrease substantially with increasing L. This is consistent with previous works [16,17,37,38] that found extremely broad distributions for the matrix elements of local operators among MBL eigenstates. On looking at the relaxation more thoroughly, we find that in this MBL regime the strongest contribution to the relaxation actually involves a set of four eigenstates, at least two of which are involved in a many-body near-resonance, as we will now describe in more detail.

Near-resonant eigenstate set.—Deep in the MBL regime, we typically find that the strongest contributions to the relaxation of $\hat{\tau}_S$ come from a set of four eigenstates, which include a near-resonant pair $|A\rangle$, $|B\rangle$ (we explain what "near-resonant" means below). The other two eigenstates involved are obtained by "flipping" the ℓ bit $\hat{\tau}_L$ adjacent to the bath:

$$|A'\rangle = \hat{\tau}_L^x|A\rangle, \qquad |B'\rangle = \hat{\tau}_L^x|B\rangle. \qquad (6)$$

In some cases, $|A'\rangle$ and $|B'\rangle$ are also near-resonant, as we discuss in the SM [35] with details. The polarization $c_A = \langle A|\hat{\tau}_S|A\rangle$ of the slow mode differs substantially between the "A" eigenstates ($|A\rangle$ and $|A'\rangle$) and the "B" eigenstates, while it is essentially unchanged by flipping $\hat{\tau}_L$, so $c_A \cong c_{A'}$ and $c_B \cong c_{B'}$. Thus, it is the transitions between $\{A, A'\}$ eigenstates and $\{B, B'\}$ eigenstates that relax $\hat{\tau}_S$. If we "demix" [16] the near-resonance to make a more localized (less entangled, more polarized) pair of orthonormal states $|a\rangle$, $|b\rangle$, we obtain

$$|A\rangle \cong |a\rangle - \epsilon|b\rangle, \qquad |B\rangle \cong |b\rangle + \epsilon|a\rangle, \qquad (7)$$

where $|a\rangle$ and $|b\rangle$ differ by spin flips at a nonzero fraction of all sites, including the sites that are most polarized in $\hat{\tau}_S$, so this is a long-range many-body resonance, in that sense, and it includes a "flip" of $\hat{\tau}_S$. The spin that is flipped between $|a\rangle$ and $|b\rangle$ that is closest to the bath is at site x. For the largest L that we can access, the most probable location of x is near $x/L = 0.8$ [35].

In the regime near the estimated avalanche instability, the "mixing" ϵ in the near-resonance is typically exponentially small in L, although it is exponentially larger than the mixing between other typical pairs of eigenstates that differ over a similar distance range. This is why we say "near-resonance": the mixing is relatively strong, partly due to the two eigenstates being near degeneracy in the spectrum of $\hat{U}_F$, but it is not fully resonant, since $\epsilon \ll 1$.

In many samples, $\{A', B'\}$ is not near-resonant and these states are well-approximated by $|A'(B')\rangle \cong \hat{X}_L|a(b)\rangle$. As a consequence of the near-resonance between $\{A, B\}$, i.e., the relatively large ϵ compared to other pairs of states, there are anomalously large matrix elements $|\langle A(B)|\hat{E}_{1,2}|B'(A')\rangle|^2 \cong \epsilon^2$ of the two jump operators $\hat{E}_{1(2)} = \hat{X}_L(\hat{Y}_L)$. These drive two particularly large contributions, $D_{AB'}$ and $D_{BA'}$ (and their transposes), to the total relaxation rate of $\hat{\tau}_S$ with $S_{AB'} \cong S_{BA'} \cong 2\epsilon^2/3$.

In addition, when the near-resonance involves flipping the polarization of site L next to the bath (so $x = L$), there is another anomalously large matrix element. This time it is the matrix element $|\langle A|\hat{Z}_L|B\rangle|^2 \cong 4\epsilon^2$ of the jump operator $\hat{E}_3 = \hat{Z}_L$ between the two near-resonant eigenstates themselves. This results in $S_{AB} \cong 4\epsilon^2/3$ and $D_{AB} \cong 2D_{AB'(BA')}$ (and its transpose).

Thus, there are two cases for $D_{\mu\nu}$, the largest contribution to Eq. (5), corresponding to whether or not the resonance involves flipping the spin nearest to the bath. The bath can drive relaxation of the slowest mode through a resonance indirectly (with X and Y jump operators), i.e., the pairs of eigenstates involved are not the near-resonant pair, and sometimes directly (with Z jump operator). We depict the two cases in Figs. 3(a) and 3(b) and call them the "XY" and "Z" cases. Our claim is that the relaxation of the slowest mode, and thus the avalanche, proceeds via these dominant processes involving four eigenstates that include a particularly strong near-resonance, as explained in this section. This structure implies that the largest contribution $D_{\mu\nu}$ comes from *either* the Z jump operator or the X and Y jump operators of the bath, depending on which of the above cases is relevant. In the Z case, which is $x = L$, the largest contribution (A-B pair) is accompanied by two XY contributions of half the magnitude (A-B' and B-A' pairs). In the XY case, which is $x < L$, there are two roughly equal largest contributions (A-B' and B-A'). In both cases, the largest contribution $D_{\mu\nu}$ doesn't exceed half of the total relaxation. The phenomenology of the near-resonant eigenstate set explained in this section is corroborated by
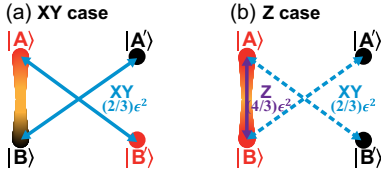
FIG. 3. Two distinct cases for the set of four most important eigenstates of $\hat{U}_F$ for the avalanche to propagate. The near-resonant pair $\{A, B\}$ are coupled with $\hat{X}_L$ and $\hat{Y}_L$ jump operators to B' and A', respectively, i.e., they have anomalously large matrix elements. In the Z case (b), the near-resonant pair involves a spin flip next to the bath (site L), and the bath can additionally couple the resonant pair with the $\hat{Z}_L$ jump operator with matrix element S_{AB} twice as large as $S_{A'B}$ and $S_{AB'}$. The two states with the largest $D_{\mu\nu}$ are colored red. In the XY case (a), this pair is not the near-resonant pair, and $\{\mu, \nu\} = \{A, B'\}$, while they are the same in the Z case, so $\{\mu, \nu\} = \{A, B\}$. In some samples, $\{A', B'\}$ are also near-resonant (not shown).

numerical observations in the next section. An extension of this simple description is discussed in the SM [35].

Numerical observations.—We numerically determine the eigenstates of $\hat{U}_F$, the slowest mode of S, and the contributions D_{mn} to its relaxation rate associated with probability currents between eigenstates. We examine the pairs of eigenstates that contribute the most ($|\mu\rangle$ and $|\nu\rangle$), identify the four important eigenstates discussed earlier, and quantify how they are related to each other to verify that the near-resonant set of eigenstates does indeed have that structure.

Recall that in our model, the polarization has a preferred spin direction: Z. Deep in the MBL regime, the local ℓ-bit operators typically are very close to the local single-spin Pauli operators. Therefore, we identify $|\gamma'\rangle \equiv \tau_L^x |\gamma\rangle$ for $\gamma \in \{\mu, \nu\}$ simply by finding the eigenstate with largest $|\langle\gamma|\hat{X}_L|n\rangle|$ among all eigenstates $|n\rangle$.

To determine which jump operator from the bath dominantly couples $|\mu\rangle$ and $|\nu\rangle$ we define a tool $Z_{\text{jump}}(m, n) := |\langle m|\hat{Z}_L|n\rangle|^2 / \sum_{j=1}^{3} |\langle m|\hat{E}_j|n\rangle|^2$. Note that $\hat{E}_3 = \hat{Z}_L$. We find that $Z_{\text{jump}}(\mu, \nu)$ is extremely close to 0 or 1 in any one sample, as shown in the inset of Figs. 4(a) and 4(b). This separation is captured by the minimal model since $Z_{\text{jump}}(\mu, \nu) \cong 0$ (or 1) is associated to the XY (or Z) case where the pair $\{\mu, \nu\}$ is not (or is) the near-resonant pair $\{A, B\}$. We therefore identify the near-resonant pair for each sample based on the minimal model as follows. In the case that $|\mu\rangle$ and $|\nu\rangle$—the pair with the largest D_{mn}—is "connected" with Z ($Z_{\text{jump}} \cong 1$), these states are identified as $|A\rangle$ and $|B\rangle$. Otherwise, if they are connected with X and Y instead ($Z_{\text{jump}} \cong 0$), we associate $\{|A\rangle, |B\rangle)\}$ to $\{|\mu'\rangle, |\nu\rangle\}$ or $\{|\mu\rangle, |\nu'\rangle\}$, whichever pair has the smaller quasienergy splitting.

We first checked that $c_\gamma \cong c_{\gamma'}$ indeed holds for $\gamma \in \{A, B\}$. This relation is satisfied because $S_{\gamma'\gamma}$ is of order 1, so the slow mode $\hat{\tau}_S$ contains negligible population
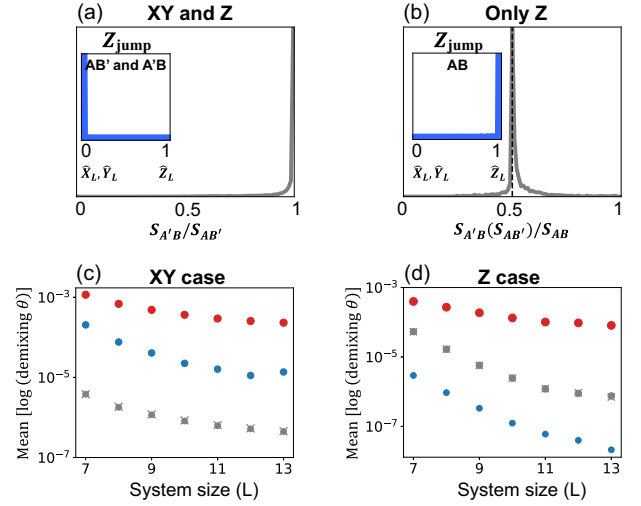

FIG. 4. Consistency with the near-resonant eigenstate set. All data here are for $\alpha = 30$. (a) The near-resonance between $\{A, B\}$ causes the AB' and $A'B$ matrix elements to be roughly equal, as described in the minimal model. The distribution of $S_{AB'}/S_{A'B}$ is indeed peaked near 1. The inset shows Z_{jump} of AB' and $A'B$ are peaked at zero (coupled with $\hat{X}_L$ and $\hat{Y}_L$). (b) When the near-resonant pair involves the spin flip of the last site (Z case), the bath can directly couple $\{A, B\}$. The distribution of the shown ratio of matrix elements demonstrates that $S_{AB} \simeq 2S_{AB'} \simeq 2S_{A'B}$. The inset shows Z_{jump} of AB is peaked at 1, implying $\{A, B\}$ are coupled with $\hat{Z}_L$. The bottom two panels show the demixing angles for (c) the XY case and (d) the Z case. The points correspond to AB (red), $A'B$ (gray ×), AB' (gray dot), and $A'B'$ (blue). The near-resonant pair identified as in the main text (AB) has the largest demixing angles for all cases. The calculations in (a),(b) are done with $L = 11$ and 10^4 disorder realizations.

difference between γ and γ'. Also, we checked that $|c_\mu - c_\nu|$ is of order 1, which should be true as we picked the pair with the largest $D_{\mu\nu} = S_{\mu\nu}(c_\mu - c_\nu)^2$. Therefore, the matrix elements S_{mn} [Eq. (3)] are a good proxy for D_{mn} [Eq. (4)] within this set of important eigenstates. We compare these matrix elements to confirm the results are consistent with the minimal model described in Figs. 3(a) and 3(b). As we show in Fig. 4(a), $S_{AB'} \cong S_{BA'}$ holds (and their transposes), and XY jump operators couple them (inset). Furthermore, when $x = L$, we additionally observe $S_{AB} \cong 2S_{AB'} \cong 2S_{BA'}$ as presented in Fig. 4(b) and $\{A, B\}$ is coupled with $\hat{Z}_L$ (inset). We note that both cases satisfy $R < 1/2$.

We finally tested our picture using the "demixing" procedure of Ref. [16], calculating the most localized basis of a subspace spanned by *two* eigenstates, and the corresponding basis rotation. The basis rotation corresponds to a location on a Bloch sphere; the polar angle, called the "demixing angle," is a measure of the resonance strength between the two eigenstates [ϵ in Eq. (7)]. As shown in Figs. 4(c) and 4(d), the demixing angle between the eigenstates we identified as $\{A, B\}$ is by far the largest among other pairs in our eigenstate set, consistent with the

idea that that pair is indeed a near-resonance that enables the bath to relax the slowest mode, i.e., the avalanche to propagate.

Conclusion.—Our Letter bridges the two key ingredients that destabilize many-body localization—*many-body resonances* and the *avalanche instability*—demonstrating that avalanches spread primarily by strong rare near-resonances. Assuming the avalanche has proceeded for a sufficiently large distance, we model the putative thermal bubble as an infinite Markovian bath with infinite temperature. In this model, we discovered the existence of dominant processes in the avalanche, involving only a few pairs of eigenstates of the closed system, including a strong near-resonance. The avalanche proceeds through these rare eigenstate pairs, leveraging many-body near-resonances to relax the spins some distance away along the chain. The inner structure of the dominant set of eigenstates is dictated by whether or not the associated resonance involves flipping a spin at the site next to the bath. This sets what jump operators effectively use the resonance present in the closed system to spread the avalanche. We presented a minimal model involving two near-resonant eigenstates and two additional auxiliary states to explain how this works in detail, and verified our picture with numerical observations. Our Letter advances the understanding of the avalanche instability of many-body localization and provides a detailed connection to rare many-body resonances present in MBL systems. Some further discussion of our conclusions and model assumptions is provided in the SM [35].

[1] P. W. Anderson, Absence of diffusion in certain random lattices, Phys. Rev. 109, 1492 (1958).

[2] D. M. Basko, I. L. Aleiner, and B. L. Altshuler, Metal-insulator transition in a weakly interacting many-electron system with localized single-particle states, Ann. Phys. (Amsterdam) 321, 1126 (2006).

[3] Vadim Oganesyan and David A. Huse, Localization of interacting fermions at high temperature, Phys. Rev. B 75, 155111 (2007).

[4] Rahul Nandkishore and David A. Huse, Many-body localization and thermalization in quantum statistical mechanics, Annu. Rev. Condens. Matter Phys. 6, 15 (2015).

[5] Wojciech De Roeck and John Z. Imbrie, Many-body localization: Stability and instability, Phil. Trans. R. Soc. A 375, 20160422 (2017).

[6] Fabien Alet and Nicolas Laflorencie, Many-body localization: An introduction and selected topics, C. R. Phys. 19, 498 (2018).

[7] Dmitry A. Abanin, Ehud Altman, Immanuel Bloch, and Maksym Serbyn, Colloquium: Many-body localization, thermalization, and entanglement, Rev. Mod. Phys. 91, 021001 (2019).

[8] Maksym Serbyn, Z. Papić, and Dmitry A. Abanin, Local Conservation Laws and the Structure of the Many-Body Localized States, Phys. Rev. Lett. 111, 127201 (2013).

[9] David A. Huse, Rahul Nandkishore, and Vadim Oganesyan, Phenomenology of fully many-body-localized systems, Phys. Rev. B 90, 174202 (2014).

[10] Anushya Chandran, Isaac H. Kim, Guifre Vidal, and Dmitry A. Abanin, Constructing local integrals of motion in the many-body localized phase, Phys. Rev. B 91, 085425 (2015).

[11] John Z. Imbrie, Valentina Ros, and Antonello Scardicchio, Local integrals of motion in many-body localized systems, Ann. Phys. (Berlin) 529, 1600278 (2017).

[12] Wojciech De Roeck and François Huveneers, Stability and instability towards delocalization in many-body localization systems, Phys. Rev. B 95, 155129 (2017).

[13] Thimothée Thiery, François Huveneers, Markus Müller, and Wojciech De Roeck, Many-Body Delocalization as a Quantum Avalanche, Phys. Rev. Lett. 121, 140601 (2018).

[14] Thimothée Thiery, Markus Müller, and Wojciech De Roeck, A microscopically motivated renormalization scheme for the MBL/ETH transition, arxiv:1711.09880.

[15] Alan Morningstar, David A. Huse, and John Z. Imbrie, Many-body localization near the critical point, Phys. Rev. B 102, 125134 (2020).

[16] Alan Morningstar, Luis Colmenarez, Vedika Khemani, David J. Luitz, and David A. Huse, Avalanches and many-body resonances in many-body localized systems, Phys. Rev. B 105, 174205 (2022).

[17] David M. Long, Philip J. D. Crowley, Vedika Khemani, and Anushya Chandran, Phenomenology of the prethermal many-body localized regime, arxiv:2207.05761.

[18] David J. Luitz, François Huveneers, and Wojciech De Roeck, How a Small Quantum Bath Can Thermalize Long Localized Chains, Phys. Rev. Lett. 119, 150602 (2017).

[19] Marcel Goihl, Jens Eisert, and Christian Krumnow, Exploration of the stability of many-body localized systems in the presence of a small bath, Phys. Rev. B 99, 195145 (2019).

[20] P. J. D. Crowley and A. Chandran, Avalanche induced coexisting localized and thermal regions in disordered chains, Phys. Rev. Res. 2, 033262 (2020).

[21] Dries Sels, Bath-induced delocalization in interacting disordered spin chains, Phys. Rev. B 106, L020202 (2022).

[22] Yi-Ting Tu, DinhDuy Vu, and S. Das Sarma, Avalanche stability transition in interacting quasiperiodic systems, Phys. Rev. B 107, 014203 (2023).

[23] Julian Léonard, Sooshin Kim, Matthew Rispoli, Alexander Lukin, Robert Schittko, Joyce Kwan, Eugene Demler, Dries Sels, and Markus Greiner, Probing the onset of quantum

avalanches in a many-body localized system, Nat. Phys. **19,** 481 (2023).

[24] Sarang Gopalakrishnan, Markus Müller, Vedika Khemani, Michael Knap, Eugene Demler, and David A. Huse, Low-frequency conductivity in many-body localized systems, Phys. Rev. B **92,** 104202 (2015).

[25] Philip J D Crowley and Anushya Chandran, A constructive theory of the numerically accessible many-body localized to thermal crossover, SciPost Phys. **12,** 201 (2022).

[26] Vedika Khemani, S. P. Lim, D. N. Sheng, and David A. Huse, Critical Properties of the Many-Body Localization Transition, Phys. Rev. X **7,** 021013 (2017).

[27] Vedika Khemani, D. N. Sheng, and David A. Huse, Two Universality Classes for the Many-Body Localization Transition, Phys. Rev. Lett. **119,** 075702 (2017).

[28] Scott D. Geraedts, Rahul Nandkishore, and Nicolas Regnault, Many-body localization and thermalization: Insights from the entanglement spectrum, Phys. Rev. B **93,** 174202 (2016).

[29] Benjamin Villalonga and Bryan K. Clark, Eigenstates hybridize on all length scales at the many-body localization transition, arxiv:2005.13558.

[30] S. J. Garratt, Sthitadhi Roy, and J. T. Chalker, Local resonances and parametric level dynamics in the many-body localized phase, Phys. Rev. B **104,** 184203 (2021).

[31] Marko Žnidarič, Antonello Scardicchio, and Vipin Kerala Varma, Diffusive and Subdiffusive Spin Transport in the Ergodic Phase of a Many-Body Localizable System, Phys. Rev. Lett. **117,** 040601 (2016).

[32] J. J. Mendoza-Arenas, M. Žnidarič, V. K. Varma, J. Goold, S. R. Clark, and A. Scardicchio, Asymmetry in energy versus spin transport in certain interacting disordered systems, Phys. Rev. B **99,** 094435 (2019).

[33] M. Schulz, S. R. Taylor, A. Scardicchio, and M. Žnidarič, Phenomenology of anomalous transport in disordered one-dimensional systems, J. Stat. Mech. (2020) 023107.

[34] Mark H. Fischer, Mykola Maksymenko, and Ehud Altman, Dynamics of a Many-Body-Localized System Coupled to a Bath, Phys. Rev. Lett. **116,** 160401 (2016).

[35] See the Supplemental Material at http://link.aps.org/supplemental/10.1103/PhysRevLett.130.250405 for additional details and discussions, which includes Refs. [8–10,16].

[36] David Pekker, Bryan K. Clark, Vadim Oganesyan, and Gil Refael, Fixed Points of Wegner-Wilson Flows and Many-Body Localization, Phys. Rev. Lett. **119,** 075701 (2017).

[37] Maksym Serbyn, Z. Papić, and Dmitry A. Abanin, Criterion for Many-Body Localization-Delocalization Phase Transition, Phys. Rev. X **5,** 041047 (2015).

[38] Samuel J. Garratt and Sthitadhi Roy, Resonant energy scales and local observables in the many-body localized phase, Phys. Rev. B **106,** 054309 (2022).